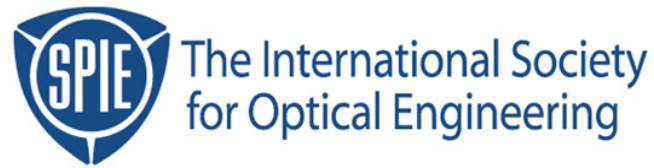


Copyright 1999 by the Society of Photo-Optical Instrumentation Engineers.



This paper was published in the proceedings of  
Optical Microlithography XII, SPIE Vol. 3679, pp. 261-276.  
It is made available as an electronic reprint with permission of SPIE.

One print or electronic copy may be made for personal use only. Systematic or multiple reproduction, distribution to multiple locations via electronic or other means, duplication of any material in this paper for a fee or for commercial purposes, or modification of the content of the paper are prohibited.

# Impact of Mask Errors on Full Chip Error Budgets

F.M. Schellenberg<sup>1</sup>, Victor Boksha<sup>1</sup>, Nick Cobb<sup>1</sup>, J.C. Lai<sup>2</sup>, C.H. Chen<sup>2</sup>, Chris Mack<sup>3</sup>

Mentor Graphics, 1001 Ridder Park Dr., San Jose, CA 95131  
WSMC, No. 25 Li-Hsin Rd., Hsinchu, Taiwan  
FINLE Technologies, P.O. Box 162712, Austin TX 78716

## ABSTRACT

As lithography pushes to smaller and smaller features under the guidance of Moore's Law, patterned features smaller than the wavelength of light must be routinely manufactured. Lithographic yield in this domain is directly improved with the application of OPC (Optical and Process Correction) to the pattern data. However, such corrections generally assume that the reticle can reproduce these features exactly. The Mask Error Enhancement Factor (MEEF) serves to amplify reticle errors, and can reduce the benefits of OPC in some circumstances. In this paper, we present the characterization of the MEEF for contact holes. These are found to have significantly higher values for the MEEF than typically measured for isolated lines. Theoretical predictions are compared with experimental results. Good agreement is found at the center of the field only when the actual area of the contact hole as formed on the reticle is used as the metric of contact size. Across field variation, however, is found to be significant requires characterization for optimum yield to be achieved.

**Keywords:** OPC, Optical Proximity Correction, MEEF, Mask Error Factor, ACLV, Optical Lithography, Yield.

## 1. INTRODUCTION

Moore's Law continues to drive developments in lithography to smaller and smaller dimensions [1][2]. OPC has been established as a fundamental requirement of sub-wavelength lithography [3], and insertion of OPC as part of the verification flow in the design data has been put forth as the optimum point of insertion for OPC [4]. The lithographic yield that can be achieved, described in more detail in the Appendix, can in principle be very high. However, the achievement of this yield improvement can be compromised by the fabrication of reticles with poor pattern fidelity.

The existence of the Mask Error Enhancement Factor (MEEF) has been discussed for some time now [5][6][7]. This description is used to describe the deviation from the ideal pattern found on the reticle, to the deviation produced in the corresponding patterning pattern on the wafer. This is mathematically expressed as

$$MEEF = \frac{\partial CD_{wafer}}{\partial (CD_{reticle} / M)} \quad [1]$$

where M is the imaging system reduction ratio (typically M=4 for DUV lithography systems). For an ideal linear imaging system, MEEF=1.0. In practice, process variables can significantly enhance the MEEF as the image fidelity of the system deteriorates.

In certain cases, particularly for isolated features, the MEEF is simply the derivative of the linearity curve [7]. We have examined this behavior experimentally, fabricating a reticle with test structures, and printing this reticle onto wafers coated with a thin oxide and 250 nm of polysilicon. Some of these wafers were then etched, allowing a comparison to be made between the reticle, resist, and etch CD. The experimental processing conditions are described in more detail below. All CD

measurements were all made using a KLA Tencor 8100-XP-R CD-SEM, which was used to measure sites within a test pattern on the reticle and the corresponding locations on wafers.

Figure 1 shows the linearity behavior for isolated lines and isolated spaces. For this particular set of experimental conditions, the process is generally linear and well behaved until below 200 nm, (although the isolated lines showed a significant etch bias) and crashes only for features smaller than 170 nm.

The corresponding MEEF is shown in Figure 2. From the figure, it is easy to conclude that, for isolated features, MEEF is not significant until features are smaller than 200 nm. Since these processes were qualified only for 250 nm features and above, this appears to represent a comfortable margin of error for this process.

## 2. THE CONTACT HOLE AS A SIMPLE CASE

In fact, these conclusions, although true for lines and spaces, are incorrect when applied to other pattern types. A case in point is the contact hole. The test patterns used to make the measurements in Figures 1 and 2 also contained isolated contact patterns, so we have evaluated their behavior in this quarter micron process as well.

The contact hole should in fact represent the simplest case for the evaluation of the MEEF. Below certain dimensions, [typically a  $k_1$  of 0.66], the radial dependence of the image of the contact no longer varies. This is because diffraction pattern of the mask is small enough that the entire pupil is filled, and the image intensity is mathematically described by the Point Spread Function of the imaging system [8]. This function, also called the Airy disk, is represented by

$$I(r) = I_0 \left[ 2 \frac{J_1 \left( 2p \frac{NA}{l} r \right)}{\left( 2p \frac{NA}{l} r \right)} \right]^2 \quad [2]$$

where  $I_0$  is the intensity at  $r=0$  and  $J_1$  is the Bessel function of the first kind of order 1, as described in standard reference materials for mathematical functions [9]. Using notation of Born & Wolf [10],  $I(r)$  has radial dependence related only to optical properties of the imaging system itself,  $\lambda$  and NA. The only variable is the maximum intensity  $I_0$ , given by

$$I_0 = E p \left( \frac{NA}{l} \right)^2 \quad [3]$$

The zero crossing point is dictated by the exposure energy required to clear the resist, which can be independently determined to provide the proportionality constant E. E is in turn related to the energy passing through the contact aperture in the reticle,

$$E \propto CD_{reticle}^2 \quad [4]$$

This leads to the transcendental equation

$$I_{threshold} = \text{constant} = K CD_{reticle}^2 p \left( \frac{NA}{l} \right)^2 \left[ 2 \frac{J_1 \left( 2p \frac{NA}{l} \frac{CD_{wafer}}{2} \right)}{\left( 2p \frac{NA}{l} \frac{CD_{wafer}}{2} \right)} \right]^2 \quad [5]$$

where K is a constant of proportionality.

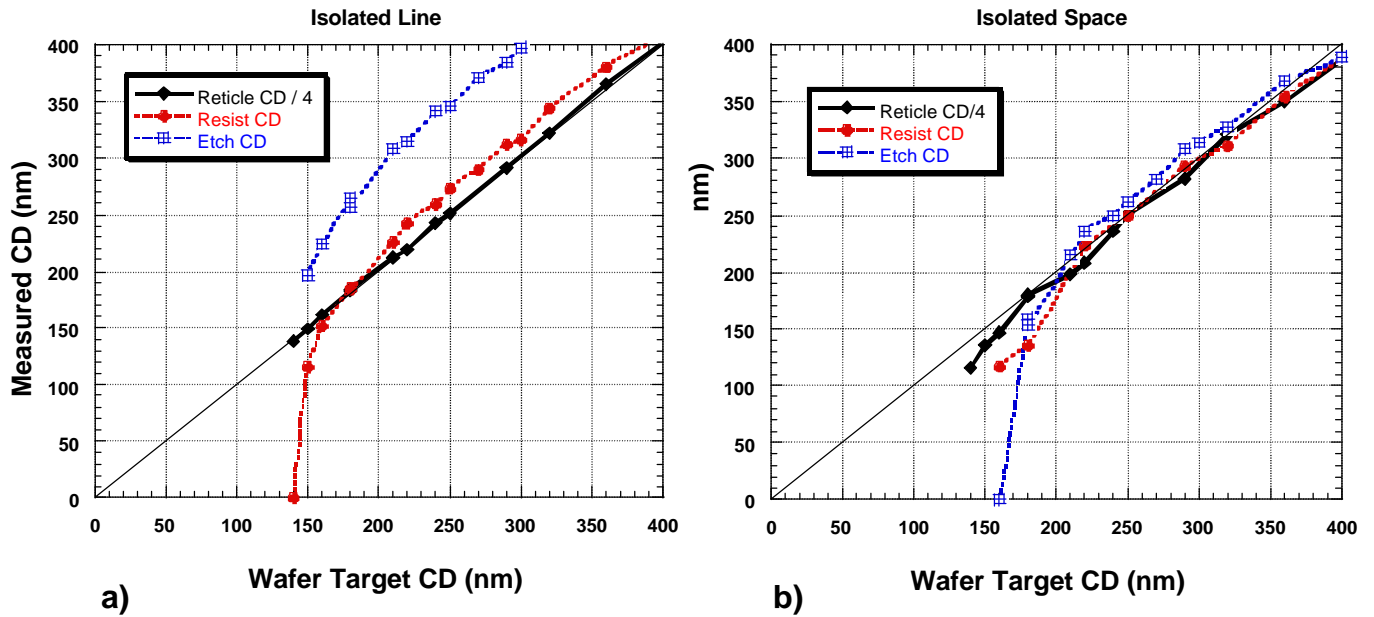


Figure 1: Linearity measurements for a) isolated lines and b) isolated spaces for the reticle used in this work, and the corresponding CDs formed on the wafer. Wafer measurements were made on fields with nominally best focus and exposure. The etch bias shown for isolated lines in a) is typical for this kind of etch process. All processes were qualified for quarter micron technology, and expected to fail for smaller dimensions.

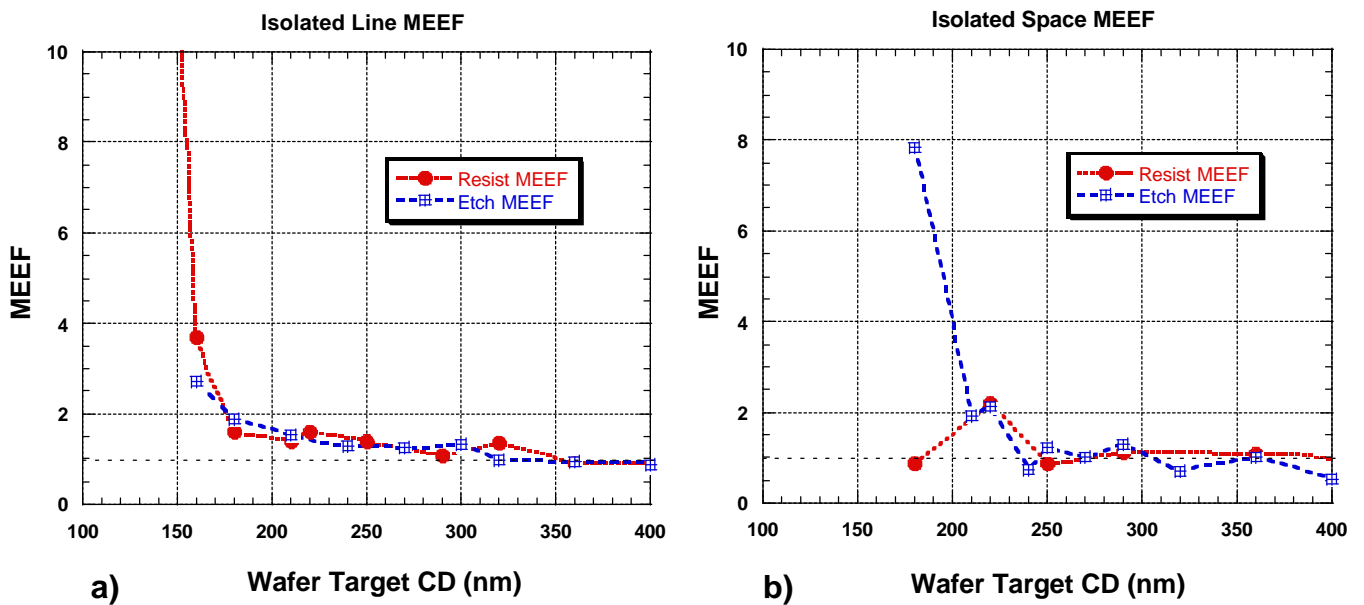


Figure 2: The MEEF data corresponding to the measured CD data in Figure 1 for a) isolated lines and b) isolated spaces.

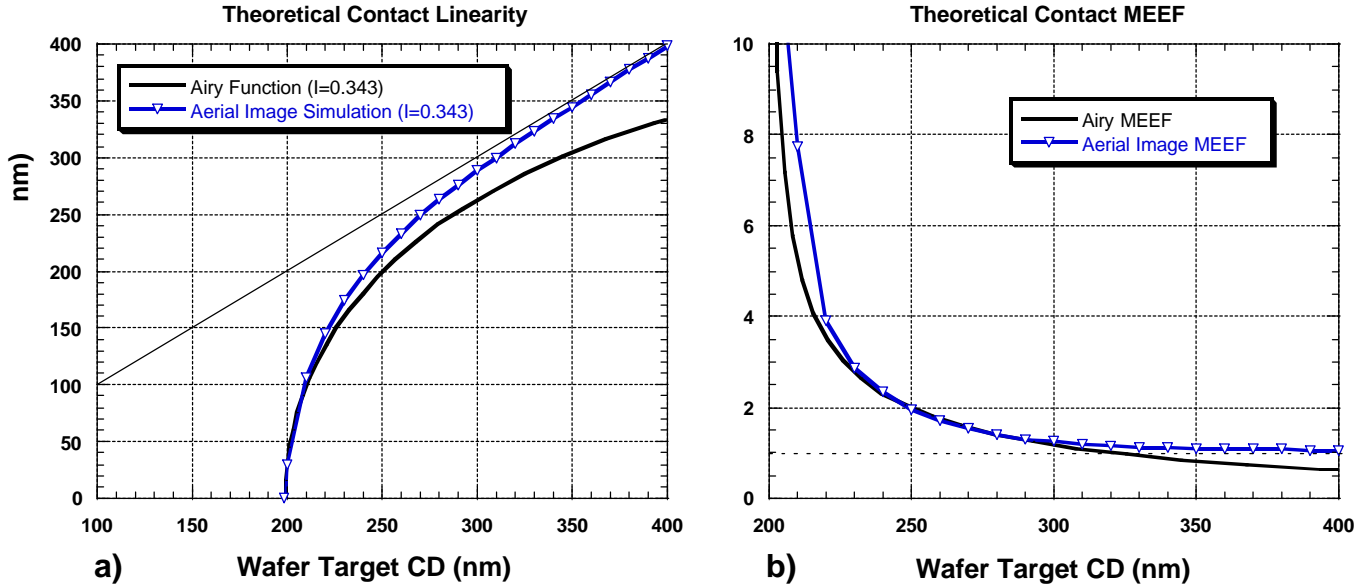


Figure 3: a) Theoretical linearity for a square contact hole, predicted by the Point Spread Function and aerial image simulation, and b) the corresponding MEEF.

Solving this transcendental equation numerically for the relationship between  $CD_{\text{mask}}$  and  $CD_{\text{wafer}}$  gives the theoretical plot shown in Figure 3a. The corresponding MEEF, found by taking the derivative of this function, is shown in Figure 3b.

A more practical method for determining this curve comes from lithographic simulation. This can be done using aerial image simulation or using full process simulation. Using the software tool PROLITH/2 [11] for the optical lithography conditions such as those described below, aerial image simulations for contact hole linearity was produced, and are also plotted in Figure 3. The agreement is very good to the ideal Point Spread Function for small contacts, diverging when  $k_1 > 0.6$ .

For small contact holes, the above theory dictates that the image of the contact is governed solely by the transmitted energy through the contact mask, which is in turn determined by the area of the contact mask pattern. This relationship can apply even for larger contact patterns. To check this more rigorously, simulations of contact hole with identical areas were simulated using five masks: a square, a diamond, a hexagon, and an octagon, and a circle. All mask designs were sized to have an area of  $(300 \text{ nm})^2$ . Aerial images were then simulated using  $NA=0.6$ ,  $\sigma=0.6$ . Simulated results at best focus are shown in Figure 4. It is clear that all images have approximately the same image width. The more circularly symmetric masks, however, produce a slightly higher peak intensity. Therefore, even for this moderately large contact hole ( $k_1=0.72$ ), mask area is still the fundamental variable controlling reticle image size.

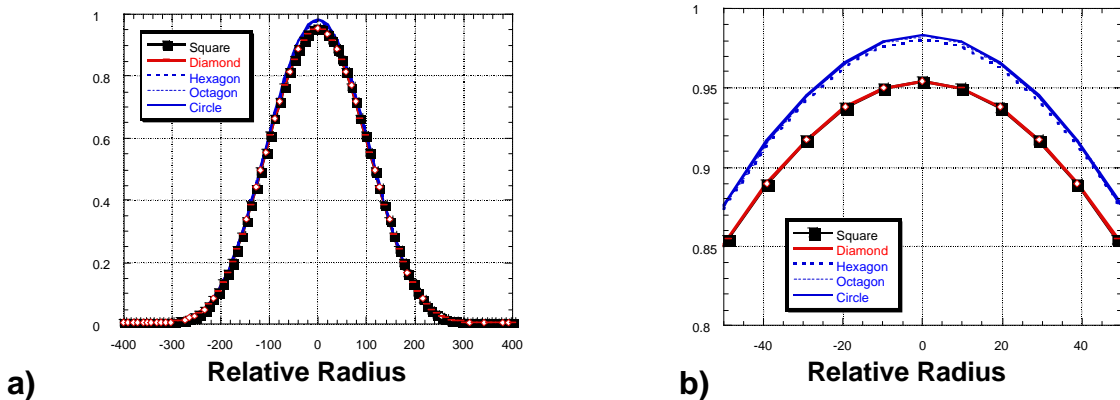


Figure 4: Aerial image simulations of contact holes with an area of  $(300 \text{ nm})^2$ , using various reticle shapes.

### 3. EXPERIMENTAL MEASUREMENTS

To make experimental measurements of the MEEF, we constructed a special reticle and processed wafers exposed using this reticle. The experimental conditions are shown below in Table I. The reticle was manufactured at DuPont Photomask using a high resolution process on a MEBES 4500 E-beam mask writer. The layout of this reticle contained multiple placements of the test structure used for generating OPC test models for the Mentor Graphics OPC product SignaMask [3] [12] [13]. The reticle was fabricated using a process qualified for quarter micron processes, and the linearity of the reticle for these features, as illustrated in Figures 1 and 2, is quite impressive.

This reticle was used to expose wafers using a Micrascan III DUV stepper at the Advanced Tool Development Facility (ATDF) at SEMATECH. Some of the wafers were then etched using a standard plasma etch process. The lithography and etch processes were only certified for quarter micron and above. Smaller features were therefore expected to fall off linearity and therefore provide an excellent opportunity for measuring MEEF data. All CD measurements were made using a KLA Tencor 8100-XP-R top-down CD-SEM. This tool is ideal for this type of metrology. The tool has the ability to measure the CD of the reticle, and to then switch to wafer mode in under a minute to allow the corresponding wafer measurements to be made. Low voltages (typically between 600V and 1 kV) are used to avoid damage to the wafer and charging distortions.

The behavior of the printed contact holes, shown in Figure 5, is significantly different than the behavior of the isolated lines and spaces. These measurements are taken from a test site near the center of the imaging field, at nominally best focus and best exposure. In all cases, the formed contacts are smaller than the target CD, and the contacts vanish altogether for dimensions below 250 nm. This is a cutoff far larger than one might be lead to believe, given the good performance of the process for isolated lines, and is even larger than the theoretical cutoff we have predicted based on aerial images. PROLITH resist simulations [11] for the contact behavior using resist properties similar to those in Table I are also shown in the figure. Although they predict a larger cutoff for the contact holes, resist behavior does not count for all the discrepancy.

The implications for the corresponding MEEF are shown in Figure 5b, calculated using  $\Delta CD_{wafer} / \Delta(CD_{mask}/4)$ . Since the process is failing for contact imaging at 250 nm, the MEEF is rising rapidly at these values – a  $k_1$  of only 0.6!. Experimentally determined values of MEEF > 4 have been presented here, with the values for the etch measurements appearing to further amplify the effect.

<b>Table I: Experimental Conditions</b>
<b>Reticle: DuPont Photomask, Round Rock, TX</b> <b>MEBES 4500 High Resolution Process</b>
<b>Wafer Processing: SEMATECH ATDF, Austin, TX</b> <b>8" wafers; 250 nm polysilicon on thin oxide</b> <b>Micrascan III Step-and-scan exposure</b> <b><math>\lambda=248</math> nm; NA = 0.6 , <math>\sigma=0.6</math> circular illumination</b> <b>UV6 resist 830 nm thick; DUV30 BARC [0.25 mm process]</b> <b>AMAT 5000 MXP Poly Etch [0.25 mm process]</b>
<b>Metrology: KLA Tencor, San Jose, CA</b> <b>8100 XP-R CD SEM</b> <b>Reticle metrology voltage 1kV,</b> <b>Wafer metrology voltage 600 V</b>

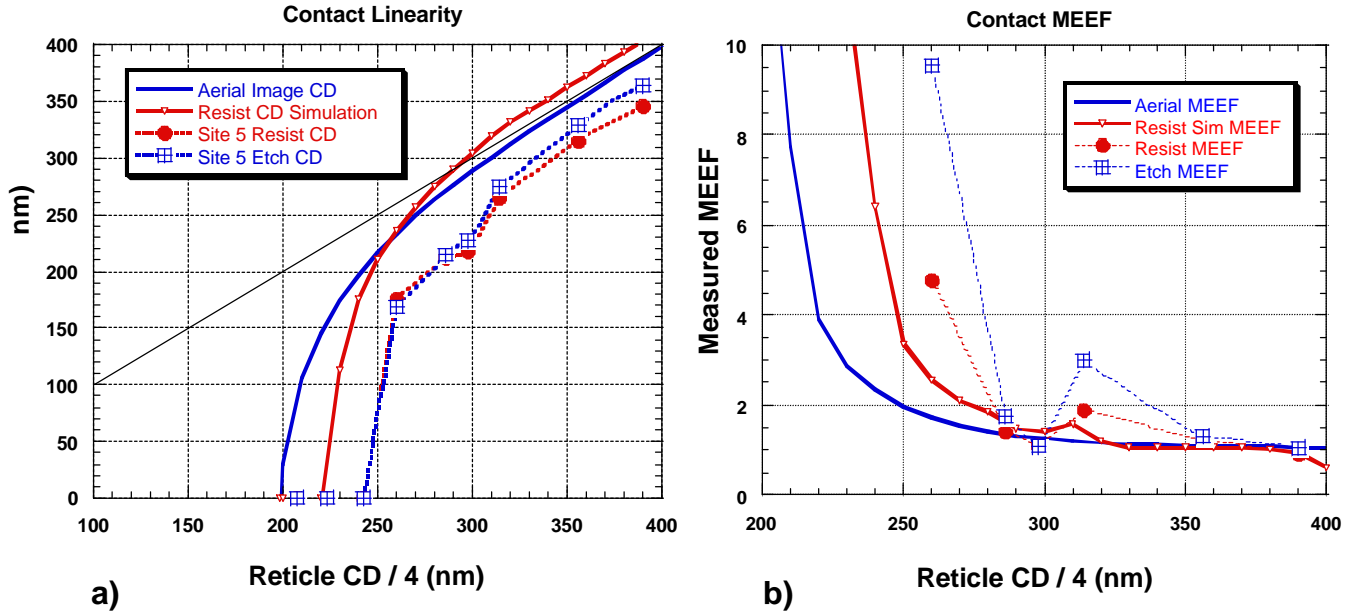


Figure 5: a) Measured linearity behavior for contact holes at the center of the exposure field, along with simulations of the image size using aerial image and resist simulations, and b) the corresponding MEEF.

The results, although agreeing qualitatively, still have a discrepancy of about 20 nm between where the cutoff is predicted and where the process actually falls. The explanation for this can be found by examining the actual contact holes formed on the reticle. As the images in Figure 6 and 7 show, larger contacts on the reticle approximate the square contact as originally drawn, with slightly rounded corners reducing the area by slightly more than 1%.

For smaller contacts, however, the contact shape is significantly distorted, as shown in Figure 7, and the energy loss is more severe. Since the image of small contact holes, as shown above, is dictated by the energy transmitted through the mask, we can take the CD-SEM image of the reticle and determine the area of the opening on the reticle using an area calculation algorithm. From this area, we can calculate the “effective” CD that a square contact that would deliver the same energy:

$$CD_{effective} = \sqrt{Area} \quad [6]$$

Values calculated in this way are shown in Table II. The energy loss, as large as 10%, is very significant. Using this equivalent CD for the reticle dimension in the X axis, the linearity curve and MEEF data become those shown in Figure 8. The agreement is much better, and any further discrepancy is certainly within experimental error and the uncertainty of the parameters used for the simulation calculations.

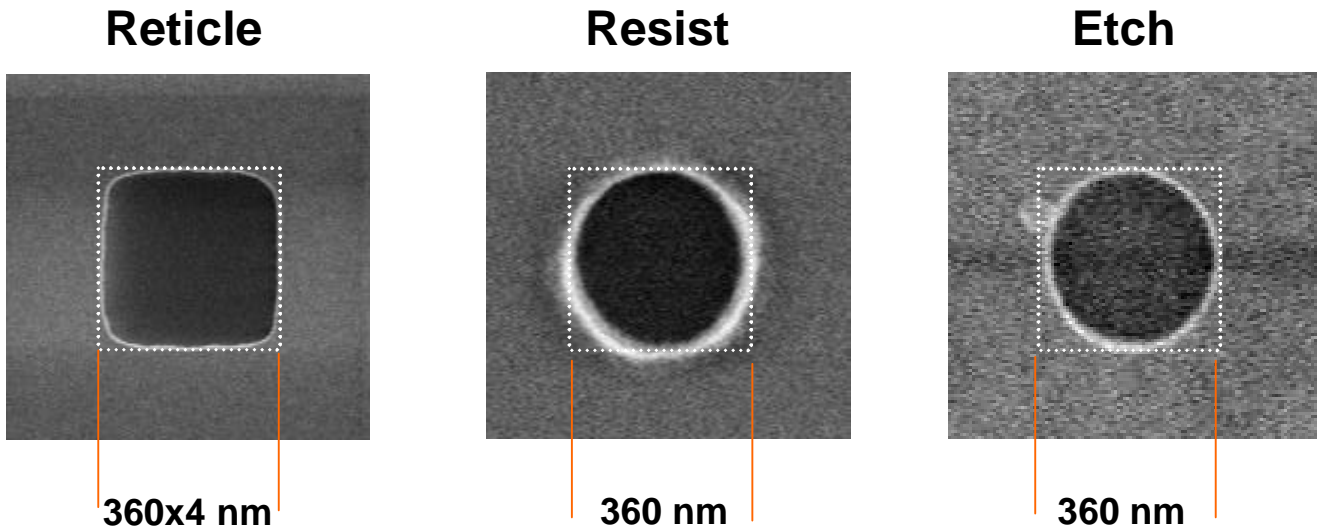


Figure 6: CD-SEM image of a contact hole on the reticle for a target wafer CD of 360 nm, and the corresponding features formed on the wafers in protoresist and after etching.

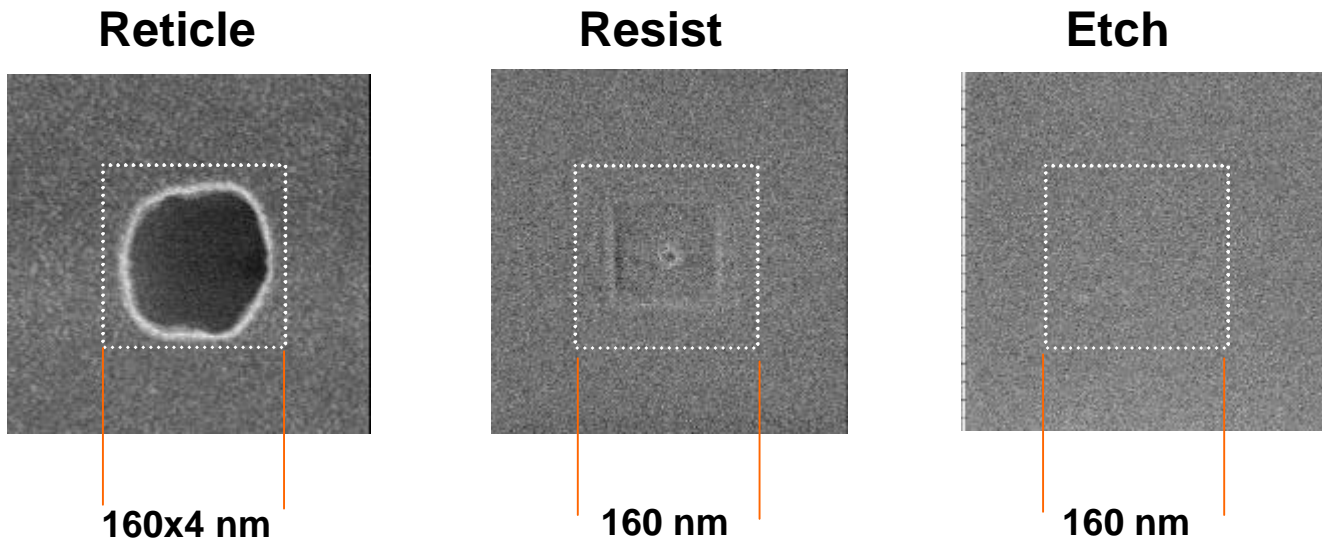


Figure 7: CD-SEM image of a contact hole on the reticle for a target wafer CD of 160 nm, and the corresponding features formed on the wafers in protoresist and after etching. The reticle deviates significantly from the drawn square shape, and no contact hole was formed on the wafer for this small dimension.

$CD_x$	Energy Ratio	$CD_{effective}$
1.0	Square: 1.00	1.0
1.0	Circle: 0.78	0.89
$CD_x(\text{nm})$	Energy ratio	$CD_{effective}(\text{nm})$
242	0.88	227
260	0.90	247
286	0.91	274
298	0.92	286
314	0.95	306
356	0.93	343

Table II: Comparison of measured x dimension CDs and the corresponding effective CD, calculated from a measurement of the area of the contact on the reticle.

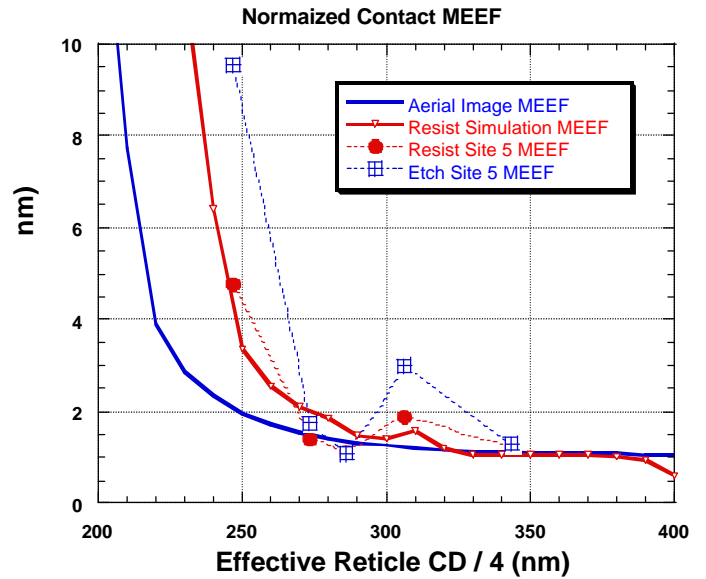


Figure 8: MEEF data as shown in Figure 5, normalized with the effective CD values in table II.

#### 4. ACROSS FIELD MEASUREMENTS

Variation of the linearity within the field is of great interest to lithographers [14] The measurements presented in the previous section were taken near the center of the lithographic field. To investigate whether these results hold throughout the field, CD SEM measurements of the reticle and the corresponding measurement sites on the resist and etched wafer were also taken for five other placements of the test pattern within the stepper field. Data from these locations are plotted together in Figure 9.

##### Resist Measurements

It is clear that there is a great deal of variation in the measurements of the contact holes in resist. For example, the contact CD with a measured reticle CD of 280 nm can form a contact with CD ranging from 150 to 240 nm depending on the location within the field – a 90nm range! Locally, however, the variation range is much better. The data for site 1&3, at the top of the field, plotted as triangles, are consistently smaller than the other contact holes from other sites.

This carries implications for the MEEF as well, plotted in Figure 9b. Although quite noisy, distinctions between the MEEF behavior for various sites can be detected. The MEEF measured for site 5, near the center of the field, is actually the smallest of the MEEF curves, while for comparison, that for sites 1&3 is significantly larger for CD values between 300 and 350 nm. The highest are observed for site 9, but only for contacts smaller than 300 nm. Note also that lithography with good linearity may also give the most dramatic MEEF behavior, as that process falls off the linearity curve. In other words, a generally well behaved process may end up having, for certain CD values, the worst MEEF values.

An illustration of the MEEF observed for these sites for 315 nm contacts is shown in Figure 10. There is not enough information here to understand whether these variations are due to systematic focus shifts, processing non-uniformities, lens aberrations, other causes, but the fact remains that there can be wide variation. If minimizing these errors in this set of measurements can serve as an example that the variation in MEEF can be extreme, and should be completely characterized if pattern fidelity and process

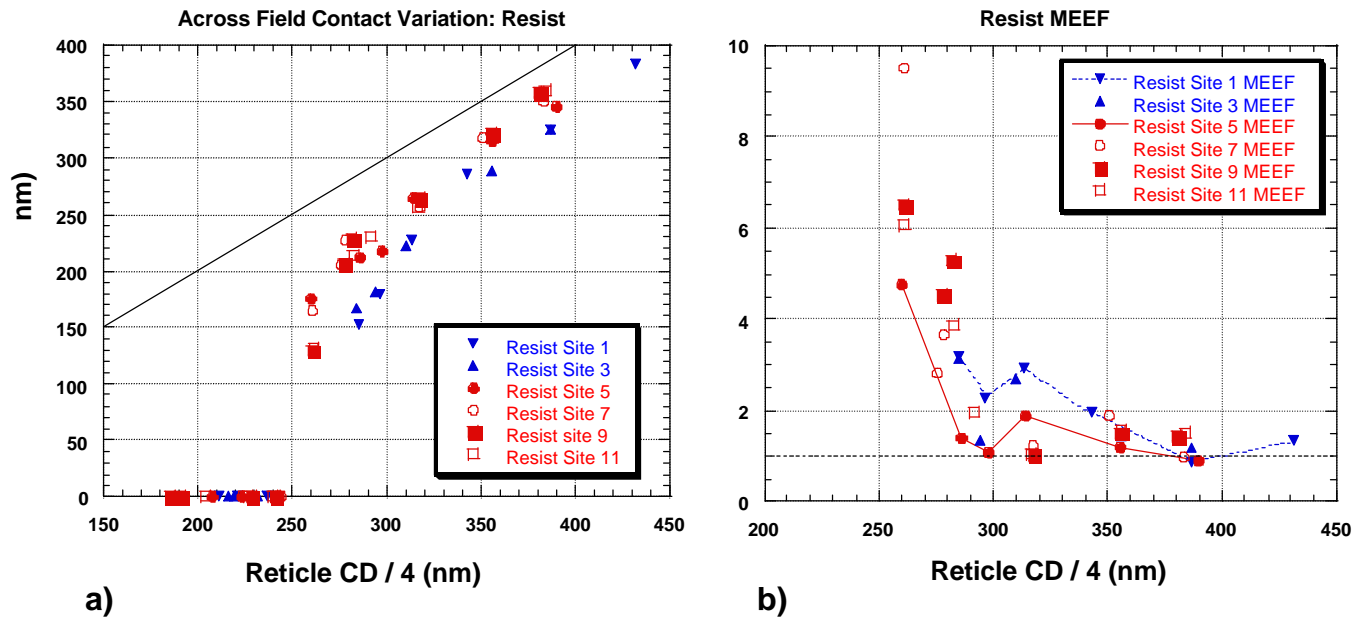


Figure 9: a) Measured linearity behavior for contact holes in photoresist at the various locations in the exposure field and b) the corresponding MEEF.

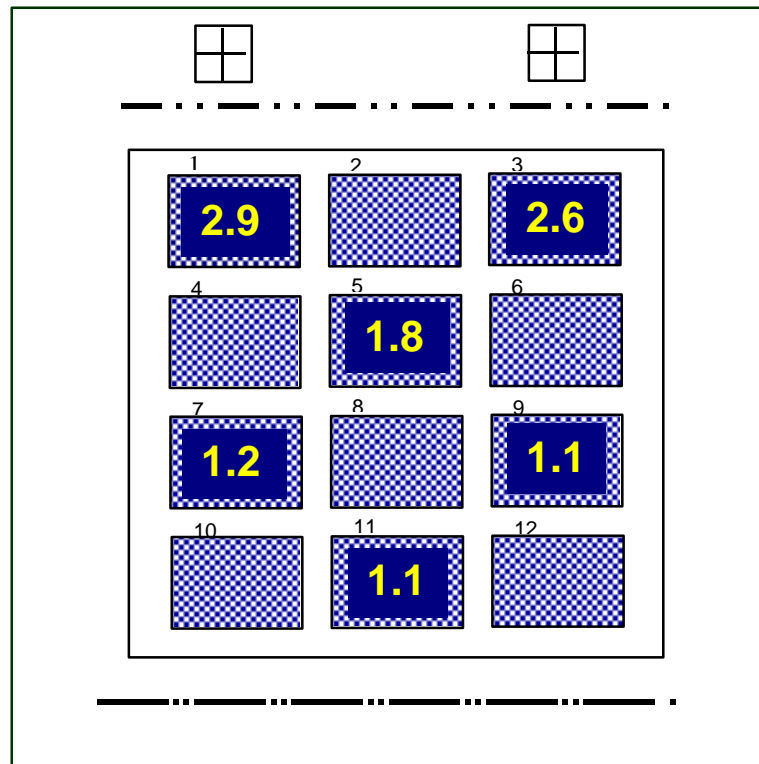


Figure 10: Schematic of the reticle layout, showing orientation and scanning marks, and the MEEF values for a 315 nm contact hole at various sites throughout the field. The MEEF values for sites 1 & 3 at the top are significantly higher than other sites in the field.

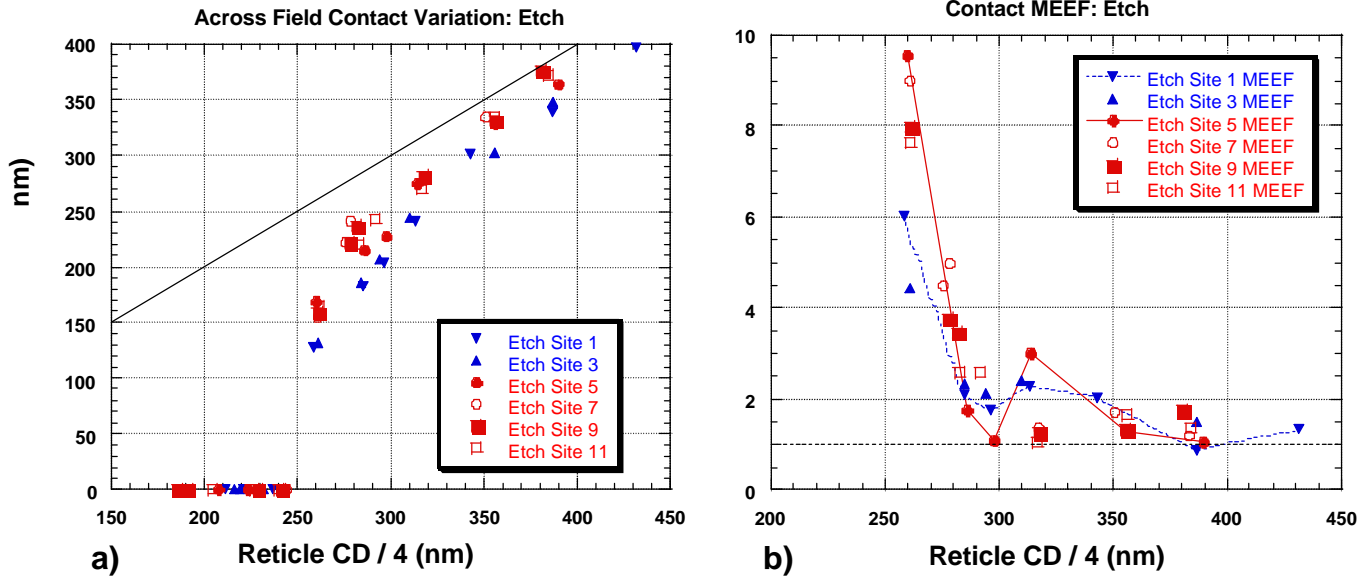


Figure 11: a) Measured linearity behavior for contact holes after etching at the various locations in the exposure field and b) the corresponding MEEF.

### Etch

The corresponding measurements of the etched features tell a slightly different story. The Etched CD measurements are shown in Figure 11a, and the corresponding MEEF in Figure 11b. Although the contacts still have a large range, the difference between sites is not as pronounced as observed in Figure 9. Site dependence of the MEEF also cannot be as easily distinguished, appearing instead to provide a random scatter around the theoretical MEEF.

This is curious, since etch processes typically are viewed as increasing randomness, and warrants further study. There could be a coincidence of cancellation between the etch process and the resist process. More likely, however, is that any etch randomization is balanced by reduced measurement uncertainty.

The aspect ratio of the contact holes formed in resist is typically near a 1:3 ratio, since the resist thickness was 830 nm, while the etched polysilicon in this experiment forms only a 1:1 ratio. Furthermore, as was illustrated in Figure 6, The images of the contact holes from the etch wafer are sharp and distinct, reflecting the good electrical conductivity of the polysilicon. This reduces the real and measurement variation due to 3D topography variations of the holes. In contrast, accurate measurements in the non-conducting photoresist are more difficult, and measuring the bottom CD of a contact hole is a notoriously difficult problem. Although the charge control mechanisms of the 8100-XP-R are excellent, mitigating these effects, and the bottom signals of the contacts were observed in this work, the photoresist measurements may still have larger variation and uncertainty. Only a larger measurement sample than that gathered here would be able to clarify this issue.

## 5. CONCLUSIONS

We have measured the MEEF for the lithography of contact holes, and found good agreement with simulated and theoretical predictions when the square root of the area of the contact as formed on the reticle is used as the equivalent reticle CD. The MEEF is significantly larger for contacts than for lines of equivalent CD, and represents a more dramatic problem for lithography. The linearity behavior, and the associated MEEF, can be different for various sites within the field, and should be characterized throughout the field for complete process optimization.

## 6. ACKNOWLEDGEMENTS

We thank Susan Macdonald and Craig West of DuPont Photomask for providing the excellent reticle used in this work; Dan Holliday, Valorie Wise-Hughes and Rich Berger for processing the wafers at SEMATECH, Geoffrey Anderson and Waiman Ng of KLA Tencor for reticle and wafer metrology; Ed Charrier for discussions on the statistical significance of data, Thuy Do and Tom Donnelly of Mentor Graphics for their assistance in building the process model used in the Appendix, Avideh Zakhor of U.C. Berkeley for helpful discussions on the use and application of OPC, and Marc Levenson for discussions on the origin and nature of the MEEF.

## 7. REFERENCES

- [1] Gordon E. Moore, "Lithography and the future of Moore's law", in Optical/Laser Microlithography VIII, Timothy A. Brunner, Ed., **Proc. SPIE Vol. 2440**, pp. 2-17 (1995).
- [2] The National Technology Roadmap for Semiconductors, 1997 Edition (Semiconductor Industry Association, San Jose, 1997)
- [3] F.M. Schellenberg, H. Zhang, and J. Morrow, "SEMATECH J111 Project: OPC Validation" in Optical Microlithography XI, Luc Van den hove, ed. **Proc. SPIE Vol. 3334**, pp 892-911, (1998)
- [4] F.M. Schellenberg, "Design for Manufacturing in the Semiconductor Industry: The Litho/Design Workshops", in Proceedings of the 12<sup>th</sup> International Conference on VLSI Design, R. Sipple, ed. (IEEE Computer Society Press, Los Alamitos, CA, 1999), pp. 111-119.
- [5] W. Maurer and D. Samuels, "Masks for 0.25-micron lithography", in Photomask and X-Ray Mask Technology, HideoYoshihara; Ed. **Proc. SPIE Vol. 2254**, (1994), p. 26-35.
- [6] W. Maurer, "Mask specifications for 193 nm lithography", in 16th Annual BACUS Symposium on Photomask Technology and Management, G.V. Shelden and J.A. Reynolds, Eds. **Proc SPIE Vol. 2884**, (1996), pp. 562-571.
- [7] C. Mack, "Mask linearity and the mask error enhancement factor", **Microlothography World**, Winter 1999 p. 11-12.
- [8] This is covered in any basic optics text, for example E. Hecht and A. Zajac, Optics (Addison Wesley, Menlo Park, CA, 1979), §11.3.
- [9] F.W.J. Olver, "Bessel Functions of Integer Order", ch. 9 of Handbook of Mathematical Functions (NBS Applied Mathematics Series 55), M. Abramowitz and I.A. Stegun, Eds. (U.S. Government Printing Office, Washington DC, 10<sup>th</sup> printing 1970).
- [10] Max Born & Emil Wolf, Principles of Optics 6<sup>th</sup> (Corrected) Edition (Pergamon Press, New York, 1980) §8.5.2, p 395 ff.
- [11] C. Mack, Inside PROLITH: A Comprehensive Guide to Optical Lithography Simulation, (Finle Technologies, Austin, TX 1997).
- [12] N. Cobb and A. Zakhor, "Fast, Low complexity mask design", in Optical/Laser Microlithography VIII, Timothy A. Brunner, Ed., **Proc. SPIE Vol. 2440**, (1995), pp. 313-327.
- [13] N. Cobb, A. Zakhor, and E. Miloslavsky, "Mathematical and CAD framework for proximity correction", in Optical Microlithography IX, Gene E. Fuller; Ed. **Proc. SPIE Vol. 2726**, (1996), p. 208-222.
- [14] O. Toublan, D. Boutin, E. Luce, and P. Schiavone, "CD Dispersion and proximity bias across the lens field characterization by electrical linewidth measurement", in Proceedings of Interface '98 Conference (1998).

## 8. APPENDIX: LITHOGRAPHIC YIELD FOR FULL CHIP OPC.

OPC is now being commonly applied to routine production of ICs for 0.25  $\mu\text{m}$  features and below. An example of the typical improvement in pattern fidelity is shown in Figure 1A and 2A. Although it is always nice to examine selected images of functioning OPC, only an evaluation of performance throughout a design presents the true evaluation of OPC efficacy.

There are many approaches to yield analysis [A1] [A2]. Simply put, these may be separated into groups related to device parameters, process parameters, and environmentally born defects. In this work we will concern ourselves with the specific version of parametric (process-related) yield and introduce the concept of lithography-related yield based on full-chip precise automated OPC ( $Y_{\text{Full\_litho}}$ ).

Lithography-related yield ( $Y_{\text{litho}}$ ) was introduced into industry vocabulary in 1994 as a metric of pattern fidelity [A3]. This is the definition we will be using in this Appendix:

$$Y_{\text{litho}} = (\text{total number of line segments within CD spec}) / (\text{total number of line segments})$$

and will extend it to account for full-chip specifics.

Another definition of  $Y_{\text{litho}}$  based on process-windows has also been suggested [A4]. This defines lithography-related yield as sum of probabilities for a CD to be within a certain process window, assuming normal and independent distributions of focus and exposure errors. While based on valid dependencies from focus and exposure, such definition depends itself on the specifics of the definition of process window shape, which can be quite complex and not well suited for easy measurement.

Because of the complexity of modern IC layouts and manufacturing process interactions, any meaningful yield estimation concept must include full-chip engine with well-established link to process details. It is no surprise, therefore, that it was impossible until the recent development of full-chip model-based automated OPC with high speed and accuracy. In our case [A5] the concept above is generalized to include pattern formation yield based not just on the formation of resist structures, but for those formed for the entire patterning process. Empirical data is gathered for features in various sizes and orientations to build a complete model. We call this  $Y_{\text{Full\_litho}}$ :

$$Y_{\text{Full\_litho}} = (\text{total number of line segments across the chip within CD spec}) / (\text{total number of line segments across the chip})$$

As an example of a calculation of  $Y_{\text{Full\_litho}}$ , we present the calculation of the improvement in line-end shortening. This situation, illustrated in Figure 3A, is usually solved by the addition of hammerheads to the line-end. The improvement that can be produced using an OPC product such as Mentor Graphics' SignaMask, as illustrated in Figure 4A, can be quite impressive. From data measured in a test pattern of our own design, a model of the total process is generated [A5][A6][A7] and then used to predict the yield expected for a representative IC design.

Figure 5Aa shows the full chip yield result predicted for a representative DUV process in use at WSMC on uncorrected pattern data. The distribution of linewidths is heavily shifted to the left, indicating average line-end shortening by 130 nm. In this case,  $Y_{\text{Full\_litho}} = 9.6\%$

Figure 5Ab shows the predicted results after OPC has been applied. The line end shortening is significantly reduced in mean and standard deviation. Nearly all the features are now within the 20 nm specification, making  $Y_{\text{Full\_litho}} = 88.4\%$

This kind of lithographic yield improvement is typical for the application of OPC. Similar order-of-magnitude results have been achieved in practice on etched wafers using this process model. However, matching specific yield predictions requires that the reticles be fabricated with the same precision that these simulations require. In practice, maskmaking remains an imperfect process, and these imperfections are magnified by the MEEF. Only when the MEEF for a process is well understood can these lithographic yields be fully realized.

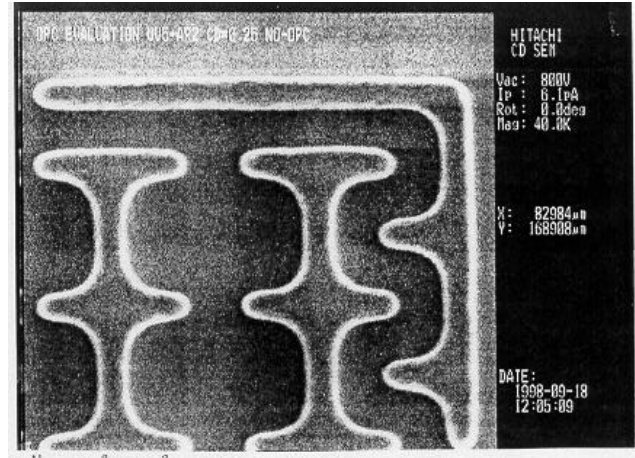
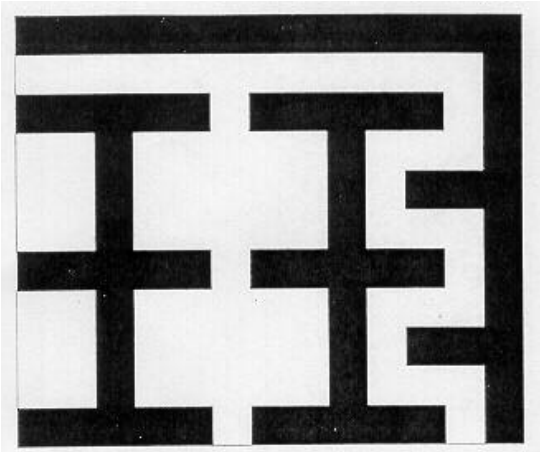


Figure 1A: a) Uncorrected design layout and b) corresponding wafer performance.

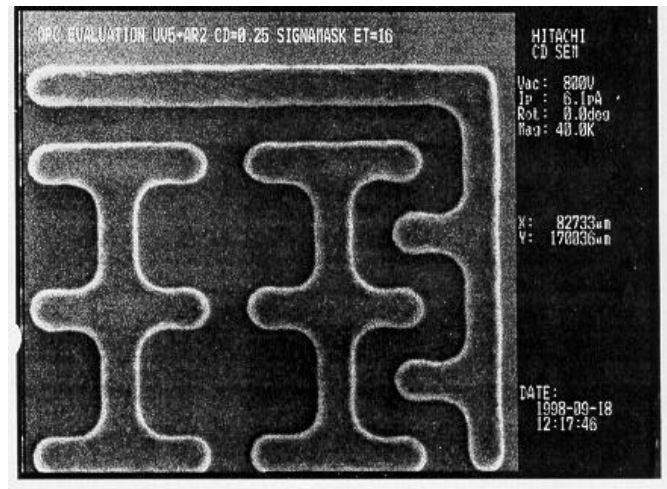
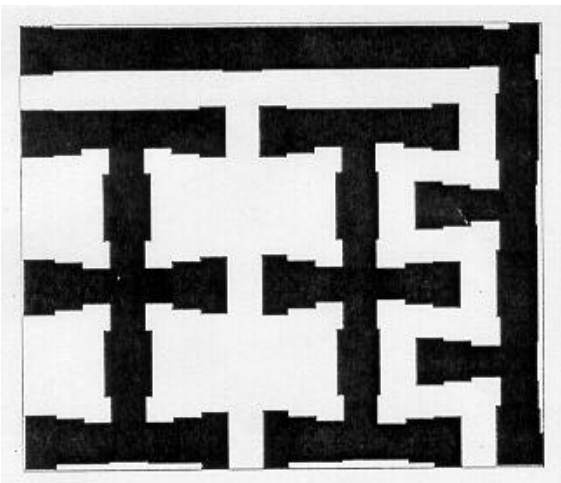


Figure 2A: a) Corrected design layout and b) corresponding wafer performance.

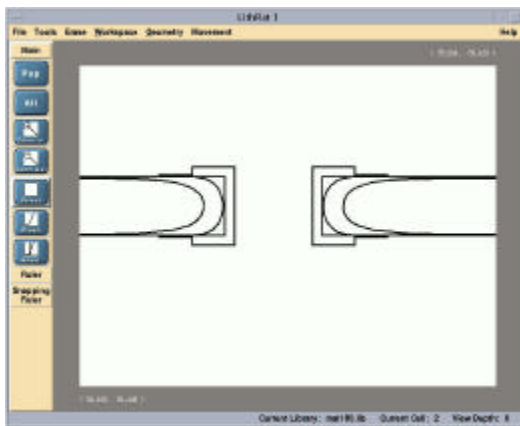


Figure 3A: Illustration of line-end shortening, both uncorrected and corrected with a hammerhead addition to the line end.

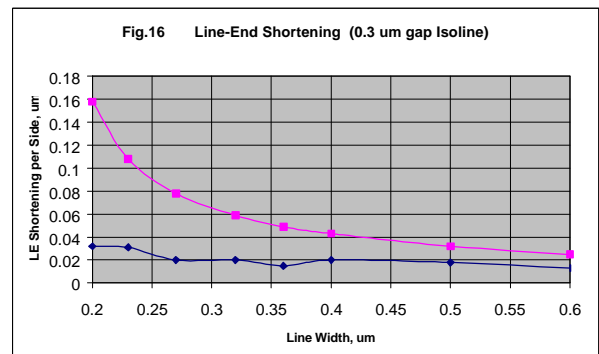
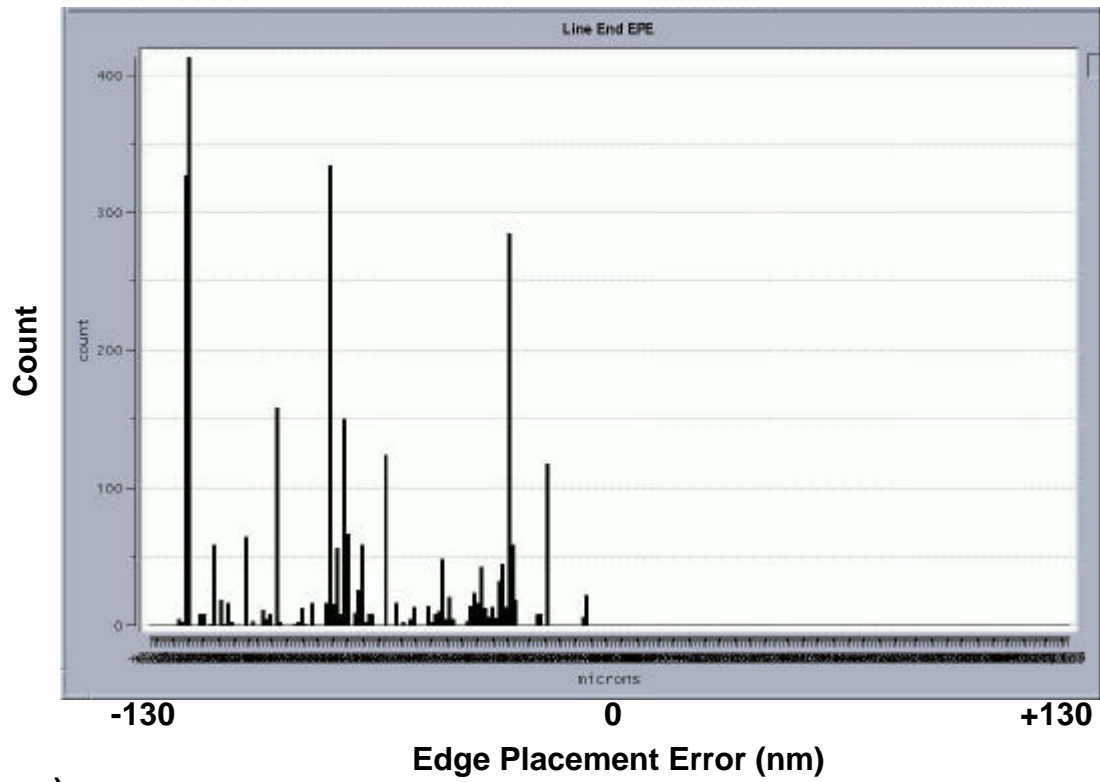
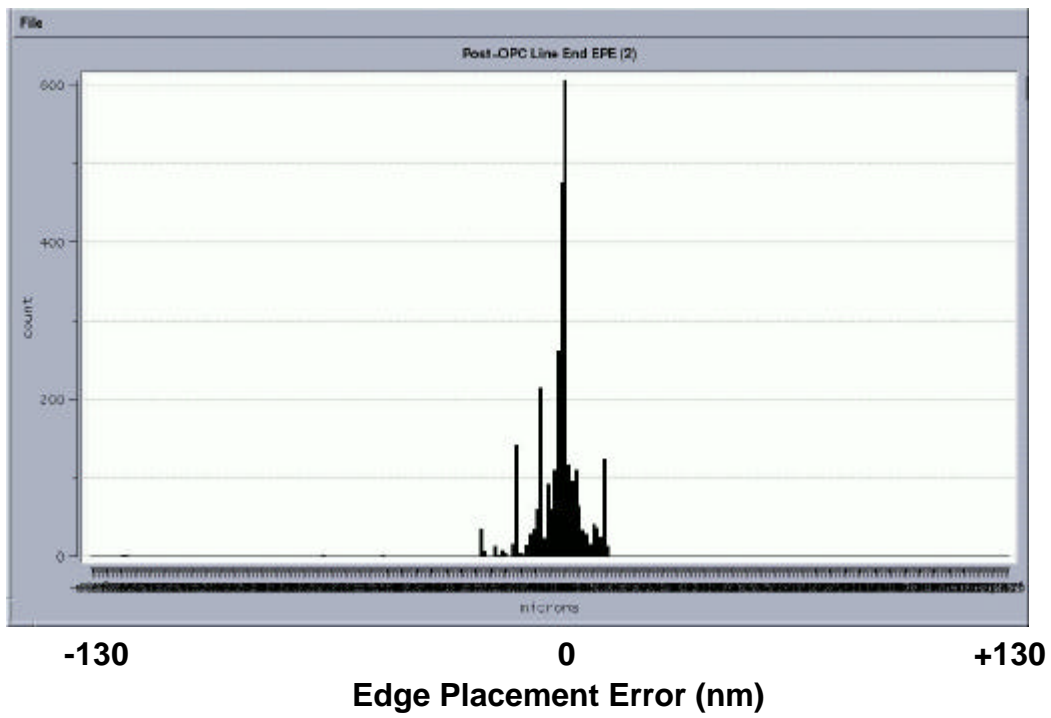


Figure 4A: Data of line end shortening, illustrating the improvement on the line end.



a)



b)

Figure 4A: a) Distribution of CDs for a WSMC quarter micron process, without OPC correction, and b) distribution after OPC has been applied.

## 9. APPENDIX REFERENCES

- [A1] C.H. Stapper, F.M. Armstrong, and K. Saji, "Integrated Circuit Yield Statistics", **Proc. IEEE** **71(4)**, April 1983.
- [A2] W. Maly, A.J. Strowjas, and S.W. Director, "VLSI yield prediction and estimation: a unified framework", **IEEE Trans. CAD of IC and Systems**, CAD-5 (1), PP. 114-130 (1986).
- [A3] Chris Mack, "Yield Modeling for Photolithography", Proceedings of the Interface '94 Conference, p. 171-182 (1994).
- [A4] A. Grassman, R. Mih, and A. Kluwe, "How focus budgets are spent: Limitations of advanced I-line lithography", in Optical Microlithography IX, Gene E. Fuller; Ed. **Proc. SPIE** **2726**, p. 386-397 (1996)
- [A5] N. Cobb and A. Zakhor, "Fast, Low complexity mask design", in Optical/Laser Microlithography VIII, Timothy A. Brunner; Ed., **Proc. SPIE Vol. 2440**, pp. 313-327 (1995).
- [A6] N. Cobb, A. Zakhor, and E. Miloslavsky, "Mathematical and CAD framework for proximity correction", in Optical Microlithography IX, Gene E. Fuller; Ed. **Proc. SPIE Vol. 2726**, p. 208-222, (1996)
- [A7] N. Cobb, and A. Zakhor, "Fast sparse aerial-image calculation for OPC", in 15th Annual BACUS Symposium on Photomask Technology and Management, Gilbert V. Shelden; James N. Wiley; Eds. **Proc. SPIE Vol. 2621**, p. 534-545 (1995)